processes

MDPI

Article

Evaluation and Improvement of the Performance of a Wellhead Multistage Bundle Gas–Liquid Separator

Xianglong Zhuge [1], Xiangdong Qi [1], Shanzhe Wang [2] and Yang Liu [1,*]

[1] Key Laboratory for Enhanced Oil & Gas Recovery of the Ministry of Education, Northeast Petroleum University, Daqing 163318, China; xianglong_zhuge@163.com (X.Z.); nepuqxd@163.com (X.Q.)
[2] Oil Recovery Plant No. 2, PetroChina Daqing Oilfield Co., Ltd., Daqing 163414, China; wangshanzhe@petrochina.com.cn
* Correspondence: lynepu@163.com; Tel.: +86-459-650-3330

Abstract: A wellhead multistage bundle gas–liquid separator combining a gas–liquid cylindrical cyclone (GLCC) with multi-tube bundle components is expected to improve the gas–liquid separation performance. However, there is no unified understanding of the factors influencing the separation performance of the separator. The continuous improvement and applications of the separator are restricted. This paper evaluated the performance of the separator using a numerical simulation method. The results indicate that the separation flow field evolves to be uniform with the increased water cut when the gas–oil ratio and flow rate remain constant. Compared with a 30% water cut, the separation efficiency at a 50% water cut increased by 5.88%. When the gas–oil ratio and water cut remained constant, the swirl effect of the primary separation was enhanced. The separation efficiency increased to more than 70% when the flow rate was 15 m/s. When the flow rate and water cut remained unchanged, the pressure of the separation flow field was reduced. However, when the gas–oil ratio was greater than 160 m^3/t, the flow field trace density of the secondary separation bundle was reduced, and the separation efficiency was also lower than 60%. The separation efficiency can be further improved by optimizing the number and diameter of secondary separation bundles.

Keywords: gas–liquid separation; gas–liquid cylindrical cyclone; separation performance; flow field characteristic; numerical simulation

Citation: Zhuge, X.; Qi, X.; Wang, S.; Liu, Y. Evaluation and Improvement of the Performance of a Wellhead Multistage Bundle Gas–Liquid Separator. *Processes* **2022**, *10*, 632. https://doi.org/10.3390/pr10040632

Academic Editors: Jui-Yuan Lee, Yufei Wang and Haoran Zhang

Received: 27 February 2022
Accepted: 23 March 2022
Published: 24 March 2022

1. Introduction

A gas–liquid cylindrical cyclone (GLCC) is widely used in oil and gas fields of different regions such as desert, land, and ocean [1,2]. Conventional volumetric separators are replaced by GLCCs with better economy and operability because a GLCC has the advantages of a simple structure, light weight, a small volume, and a wide treatment range [3–5]. In high water cut oil and gas fields, for example, during the process of oil and gas exploitation and transportation, the produced liquid often exists in the form of multiphase flow. Thus, it is easy for the produced liquid to form an unstable flow state caused by many factors, such as pressure, which increases the measurement error in the process of delivery. In order to overcome the problem of inaccurate measurement, a growing number of optimized measurement methods have appeared. Their core principle is basically similar; that is, they separate the different phases into a multiphase flow and then measure them separately [1,6–8]. The combination of a GLCC and a metering device is superior to other conventional methods. The discontinuity and instability in the metering process are overcome, and the metering of the small flow rate of the multiphase flow is realized [9–11].

However, the separation flow field inside the separator is relatively complex. During the production of oil and gas fields, the physical parameters of the recovered fluid also undergo dynamic changes, such as the water cut, gas–oil ratio, and other factors. However, since GLCC separators use gravity and centrifugal force for gas–liquid separation, slip

occurs between the gas–liquid phases due to the density difference between the gas–liquid phases, and the liquid phase is thrown against the pipe wall while the gas phase is discharged through the fixed pipe. During the separation process, when the amount of the liquid phase increases beyond the threshold of separation performance or the flow rate changes, it will adversely affect the separation effect. Therefore, traditional GLCC separators can no longer meet actual production needs [9,12]. In addition, there are also some problems in the application of a GLCC, such as the difficulty of liquid level control, eliminating slug flow, the influence of multiple factors on the separation effect, and the low accuracy of subsequent metering. These problems are improved by the wellhead multistage bundle gas–liquid separator. In the separator, efficient gas–liquid separation is realized by the GLCC and multi-tube bundle components. After the gas–liquid mixture is separated by the primary GLCC swirl, it enters the multi-tube separator for secondary deep separation. The separation efficiency is improved, and the measurement accuracy is guaranteed. Although the principle of the separator is clear, the structure is simple, and the application is convenient, the separation performance of the separator is affected not only by the geometric structure characteristics but also by the flow conditions of the gas–liquid mixture. The flow pattern and geometric parameters such as inlet inclination angle and flow rate have been researched in some studies [12,13]. For example, the internal flow behavior and gas–liquid separation efficiency of a GLCC were analyzed, and then the evaluation and optimization were realized [4,7,8,14]. However, these were only for single-stage separation optimization of GLCC, and the separation performance evaluation of the improved multistage bundle gas–liquid separator was not considered.

Therefore, the separation performance of the separator in this paper is studied by the numerical simulation method, the separation flow field and separation effect are observed, the influence law of water cut, flow rate, and gas–oil ratio of the gas–liquid mixture is explored, the gas–liquid separation process is described, the separation efficiency is quantitatively compared, the further optimization direction of separator geometric structure is proposed, and the expanded application of a GLCC is provided.

2. Model Development

2.1. Modeling of the Wellhead Multistage Bundle Gas–Liquid Separator

The wellhead multistage bundle gas–liquid separator is a skid-mounted structure, which includes a two-stage separation unit, gas flowmeter, liquid flowmeter, measurement data acquisition system, power distribution system, pipelines, and other components [15]. The gas–liquid mixture enters the GLCC through the primary separation inlet of the separator, forming a swirling flow, and the mixture is separated into a gas phase and liquid phase under the combined action of gravity, centrifugal force, and buoyancy. Then the liquid phase is agglomerated into large droplets by a swirling action, and, subsequently, affected by centrifugal force, the liquid is separated along the radial direction and collected at the bottom. Meanwhile, the remaining liquid phase is carried by the gas phase, flowing to the gas-gathering tube, and the primary separation is realized [7–10]. The gas phase enters the gas-gathering tube and continues to move upwards, passing through the gas separation elbow and the secondary separation bundle between the elbow and the gas-gathering tube; then, the deep secondary separation is carried out. After separation, the gas and liquid phases enter the different flowmeters, and the accuracy of the gas phase and liquid phase measurement can be guaranteed [14,16,17].

For the wellhead multistage bundled gas–liquid separator, the gas–liquid separation function is mainly affected by the GLCC and multi-bundle components. Therefore, according to the needs of the numerical simulation process, the separator structure is simplified in this part. The strengthening structures and auxiliary components in the separator are ignored, and the measurement and collection parts of the gas phase outlet and the lower liquid phase outlet are ignored; so, the simplified physical model of the separator is obtained, as shown in Figure 1. The geometric parameters of the separator are shown in Table 1.

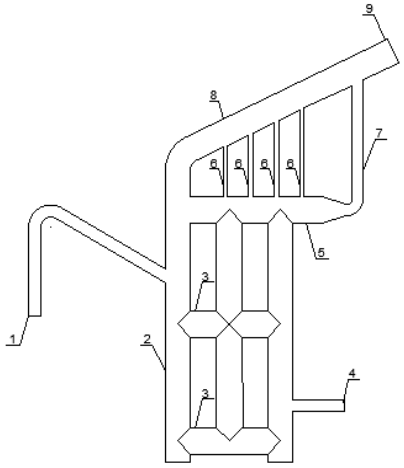

Figure 1. Simplified physical model of the wellhead multistage bundled gas–liquid separator. 1—primary separation inlet; 2—cylindrical cyclone (GLCC); 3—balance tube; 4—liquid phase outlet; 5—gas-gathering tube; 6—secondary separation bundle (thin); 7—secondary separation bundle (coarse); 8—gas separation elbow; 9—gas phase outlet.

Table 1. Geometrical parameters of the physical model.

Structure Parameters	Size, mm	Structure Parameters	Size, mm
Length of the primary separation inlet riser	500	Diameter of the primary separation inlet riser	66
Length of the primary separation inlet inclined tube	700	Diameter of the primary separation inlet inclined tube	66
Length of the cylindrical cyclone	1780	Diameter of the cylindrical cyclone	147
Length of the balance tube	1200	Diameter of the balance tube	147
Length of the liquid phase outlet	300	Diameter of the liquid phase outlet	66
Length of the gas-gathering tube	796.5	Diameter of the gas-gathering tube	147
Diameter of the secondary separation bundle (thin)	26	Diameter of the secondary separation bundle (coarse)	66

The mixture model is simplified as the Euler model, which considers the diffusion and fluctuation effect between phases and uses the concept of slip velocity to describe the phase moving at different speeds [16,18–20]. For the turbulence model, the influence of the wall surface on the Reynolds stress distribution in the Reynolds stress model (RSM) was considered, and the strong rotation motion in the flow field can be completely reproduced [18,21–23]. Therefore, the mixture model and RSM were selected.

$$\frac{\partial}{\partial t}(\rho_m) + \nabla \cdot \left(\rho_m \cdot \vec{v_m}\right) = \dot{m} \tag{1}$$

$$\rho_m = \sum_{k=1}^{n} \alpha_k \rho_k \tag{2}$$

$$\vec{v_m} = \frac{\sum_{k=1}^{n} \alpha_k \rho_k \vec{v_k}}{\rho_m} \tag{3}$$

Here, $\dot{m}$ is the mass change rate of the mixture (kg/s); ρ_m is the density of the mixture (kg/m^3); $\vec{v_m}$ is the mass average velocity of the mixture (m/s), and α_k is the volume fraction of phase k (%).

$$\frac{\partial}{\partial t}\left(\rho_m \vec{v_m}\right) + \nabla \cdot \left(\rho_m \vec{v_m} \vec{v_m}\right) = -\nabla p + \nabla \left[\mu_m \left(\nabla \vec{v_m} + \nabla \vec{v_m}^T\right)\right] + \rho_m \vec{g} + \vec{F} + \nabla \cdot \left(\sum_{k=1}^{n} \alpha_k \rho_k \vec{v_{dr,k}} \vec{v_{dr,k}}\right) \tag{4}$$

$$\mu_m = \sum_{k=1}^{n} \alpha_k \mu_k \tag{5}$$

$$\vec{v}_{dr,k} = \vec{v}_k - \vec{v}_m \tag{6}$$

Here, $\vec{F}$ is the volume force (N); μ_m is the viscosity of the mixture (Pa/s), and $\vec{vdr}, k$ is the drift velocity of phase k (m/s).

2.2. Calculating Process

In the process of primary gas–liquid cyclone sedimentation separation and secondary multi-bundle deep separation, the separator performance can be further evaluated by observing the characteristics of flow field distribution and evolution. After considering the structural and functional characteristics of the separator, the separator was divided into three parts, including the GLCC, the multi-bundle separation unit, and other parts. Then, Gambit was used to mesh with different grid densities, and the unstructured grid of the physical model was generated. As shown in Figure 2, the grid of the GLCC part was encrypted.

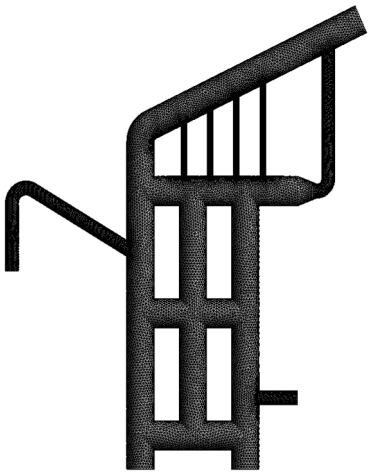

Figure 2. Mesh generation of the physical model.

The wall of the model was set to a static state, and the influence of viscosity was considered. The inlet of the incoming liquid was set to a velocity inlet, and the boundary of the separation outlet of the liquid phase and gas phase was set to a free flow outlet. The operating pressure was set based on the field practice pressure. At the same time, the droplet particle adopted the approach of surface injection, and the droplet at the nozzle of the liquid phase outlet was set as an escape; so, the separation efficiency can be expressed as Equation (7).

$$\eta = \frac{N_0 - N_r}{N_0} \times 100\% \tag{7}$$

Here, η is the separation efficiency (%); N_0 is the number of droplets at the primary separation inlet (pcs), and N_r is the number of droplets at the gas phase outlet (pcs).

In the process of the numerical scheme, the above model was considered, and some assumptions in the process of gas–liquid separation of the separator were proposed. Firstly, the separator was filled with air; then, the gas–liquid two-phase mixture entered [15,24]. In addition, in the process of gas–liquid separation, the gas–liquid two-phase mixture was an incompressible fluid, and its temperature remained unchanged [10,14].

During the gas–liquid separation process, the flow characteristics were affected by gravity, and there was mutual movement between the gas phase and the liquid phase in the gas–liquid mixture [25]. Therefore, the unsteady calculation was adopted as the calculation method, the SIMPLE algorithm was used as the numerical simulation solution, the least-squares cell-

based method was selected as the pressure gradient term, and PRESTO! was adopted as the pressure dispersion term. In terms of time discretization, the first-order implicit format was adopted, the relaxation factor of each variable was set to default, the calculation accuracy was guaranteed, and the calculation efficiency was improved [18,26–28]. Different flow conditions were simulated, and the change in the gas–liquid separation performance of the separator was observed. The specific parameter settings are shown in Table 2.

Table 2. Parameters for the simulated calculation.

Water Cut, %	Flow Rate, m/s	Gas–Oil Radio, m^3/t	Pressure, MPa
30 40 50	20	160	0.70
40	15 20 25	160	
40	20	100 160 220 280	

3. Results and Discussion

3.1. Effect of Water Cut on the Performance of GLCC

3.1.1. Pressure Distribution and Separation Flow Field

In the primary separation process, each section in the gas–liquid cylindrical cyclone (GLCC) was selected from top to bottom, and the pressure value of each section was obtained by calculation. Therefore, the axial pressure distribution in the GLCC with different water cuts was obtained.

As shown in Figure 3, the pressure distribution characteristics in the GLCC were similar under different water cuts. The curve in the figure shows the pressure distribution along the axis of the separator, and the pressure peak occurred at the inlet of the inclined tube along with the fluid entry. The pressure at the inclined tube of the primary separation inlet was the highest. As the gas–liquid mixture flowed downward, swirl separation occurred and the energy was reduced; so, the pressure value was reduced. However, with the increase in water cut, the pressure increased at the inclined tube of the GLCC, and the pressure drop required for separation also increased. The evaluation shows that the gas–oil ratio remained unchanged, and the proportion of the liquid phase was increased with the increase in water cut. Under the effect of gravity, the pressure at the inclined tube increased.

The separation flow field characteristics of the separator at different water cuts are shown in Figure 4; different colored streamlines in the figure indicate different flow trajectories in the flow field that do not intersect each other. The different colors aim solely to facilitate discrimination. The gas–liquid mixture entered the GLCC along the primary separation inlet; with the increase in water cut, the characteristics of centrifugal force generated by the swirling flow significantly improved. As a result, most of the liquid phase flowed along the radial direction of the GLCC to the tube wall and flowed downward along the tube wall; the liquid phase was discharged by the liquid phase outlet. The remaining liquid phase was carried by the gas phase and entered the gas-gathering tube through the balance tube from the center of the separation tube. The gas–liquid secondary separation was carried out in the secondary separation bundle, and the overall flow field distribution was more uniform. At the same time, with the increase in water cut, the turbulence intensity of the flow field in the balance tube and the gas-gathering tube area increased.

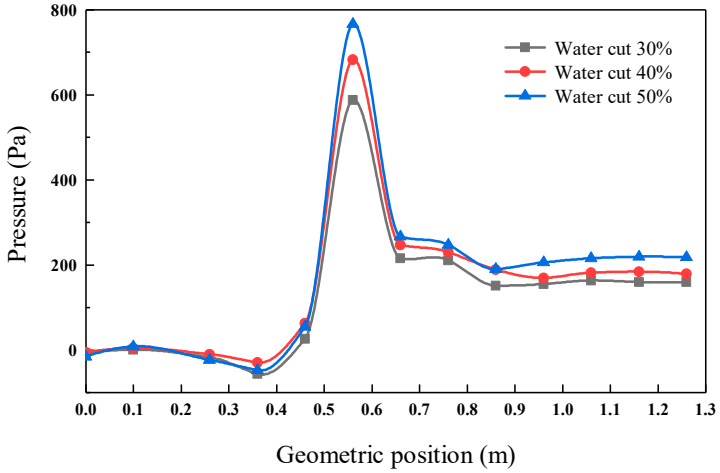

Figure 3. Effect of the water cut on the axial pressure distribution of a cylindrical cyclone.

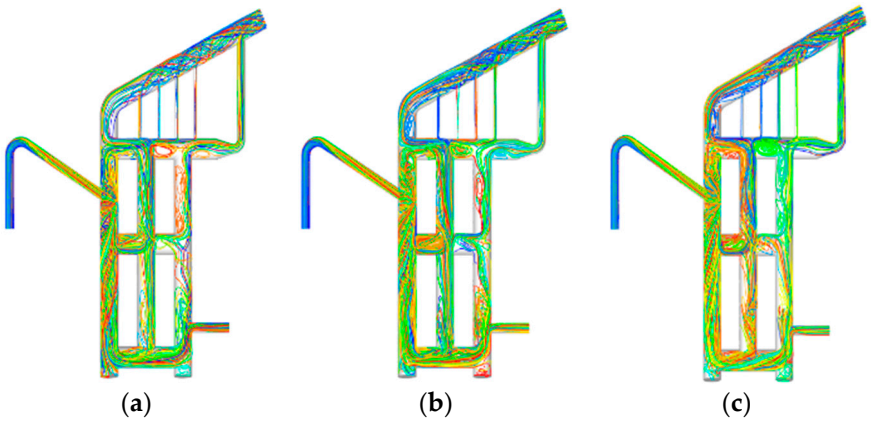

Figure 4. Effect of the water cut on the gas–liquid separation flow field characteristics. (**a**) 30%; (**b**) 40%; (**c**) 50%.

3.1.2. Separation Performance

The discrete phase model (DPM), a multiphase flow model, is widely used in numerical simulations to track the motion of particles of small content phases [29]. The DPM model was used for droplet trajectory tracking, and the capture condition of droplets by the separator was obtained; so, the separation performance was quantitatively characterized by the separation efficiency, and then the influence of subsequent measurement on the separation performance was judged. At the same time, the pressure drop between the primary separation inlet and the gas phase outlet was calculated, it can be used as the characteristic parameter of the separation pressure drop. When the separator throughput was the same, the lower the pressure drop was, the better the separation performance. The gas–liquid separation effect of the separator under the influence of water cut is shown in Table 3.

Table 3. Effect of the water cut on the gas–liquid separation performance.

Water Cut, %	Separation Efficiency, %	Separation Pressure Drop, Pa
30	64.19	2809
40	65.94	3078
50	70.07	3637

When the flow rate, gas–oil ratio, and pressure were consistent, the water cut of the gas–liquid mixture was increased from 30% to 50%, and the separation efficiency of the

separator showed a gradual upward trend; the maximum value of 70.07% was obtained when the water cut was 50%. Overall, the separation effect was consistent with the axial pressure of the GLCC and the distribution characteristics of the separation flow field. In addition, with the increase in water cut, the liquid phase proportion in the gas–liquid mixture increased, and the separation pressure drop increased.

3.2. Effect of Flow Rate on Performance of GLCC

3.2.1. Pressure Distribution and Separation Flow Field

In the primary separation process, the distribution of axial pressure in the GLCC at different flow rates was obtained by observing the cross-section from top to bottom in the GLCC.

As shown in Figure 5, at different flow rates, the pressure distribution trend of the gas–liquid mixture in the GLCC was generally similar. However, the fluctuation of the pressure distribution curve was observed, the flow rate increased, and the pressure required for swirl separation at the inlet also increased. At the same time, with the movement of the gas–liquid mixture, the area of the balance tube and gas-gathering tube was affected by the sudden increase in pressure, and the stability of the pressure was reduced.

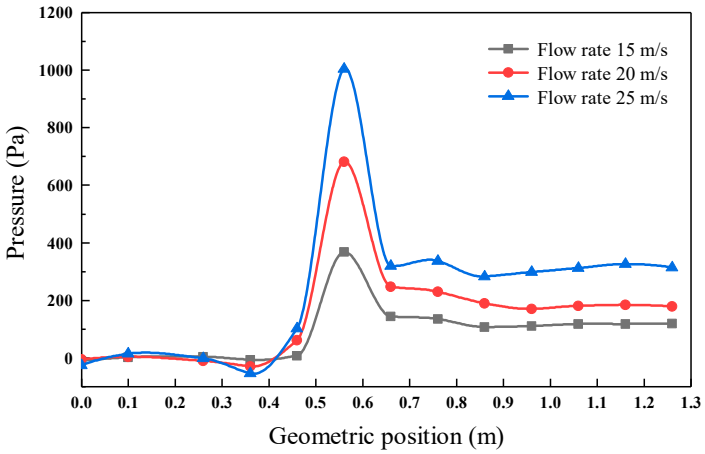

Figure 5. Effect of flow rate on the axial pressure distribution of the cylindrical cyclone.

The separation flow field characteristics of the separator at different flow rates are shown in Figure 6. It can be seen that as the flow rate increased, the swirl characteristics of the gas–liquid mixture in the GLCC were enhanced, and the irregularity of the streamline trajectory was also enhanced. The effect of the gas phase gathering and liquid phase reflux was inhibited in the secondary separation bundle. From the perspective of the flow field characteristics, the swirl action in the gas-gathering tube was more obvious, and the irregular streamline trajectory in the gas separation elbow was also obvious. The gas–liquid separation efficiency was affected by the flow field characteristics to varying degrees.

3.2.2. Separation Performance

Similar to the method for evaluating water cut, the gas–liquid separation efficiency of the separator was obtained by tracking the droplet trajectory at different flow rates. The results are shown in Table 4. The water cut of the gas–liquid mixture was set to 40%, and the gas–oil ratio was set to 160 m^3/t. Compared with the flow rate of 20 m/s and 25 m/s, a higher separation efficiency was obtained at 15 m/s. At this time, the separation efficiency was 72.35%, and the separation pressure drop was the minimum value of 1729 Pa, which was also consistent with the axial pressure and flow field distribution.

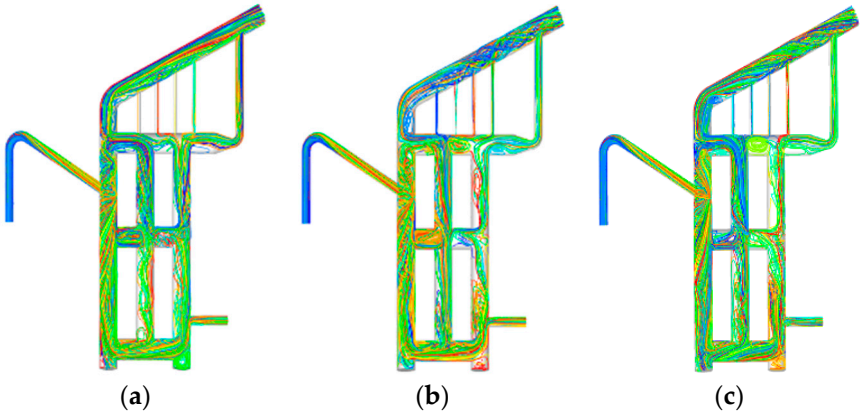

Figure 6. Effect of the flow rate on the gas–liquid separation flow field characteristics. (**a**) 15 m/s; (**b**) 20 m/s; (**c**) 25 m/s.

Table 4. Effect of the flow rate on the gas–liquid separation performance.

Flow Rate, m/s	Separation Efficiency, %	Separation Pressure Drop, Pa
15	72.35	1729
20	65.94	3078
25	61.79	4914

3.3. Effect of the Gas–Oil Ratio on the Performance of GLCC

3.3.1. Pressure Distribution and Separation Flow Field

The distribution characteristics of the axial pressure in the GLCC with different gas–oil ratios are shown in Figure 7. When the gas–oil ratio was reduced, the liquid phase proportion in the gas–liquid mixture increased; so, the pressure of the gas–liquid mixture entering the GLCC increased continuously. High pressure at the center of the separation cylinder area was generated, and the stability of the high-pressure transmission along the GLCC to the lower part became worse.

The separation flow field characteristics of the separator at different flow rates are shown in Figure 8 The gas–oil ratio increased from 100 m^3/t to 160 m^3/t, the flow field stability in the primary and secondary separation regions in the separator was improved, and the streamline distribution was dense. As the gas–oil ratio continued to increase, the flow field stability also increased. However, the flow line density in the secondary separation area was reduced significantly, the secondary separation performance was affected, and the overall separation efficiency of the separator was reduced.

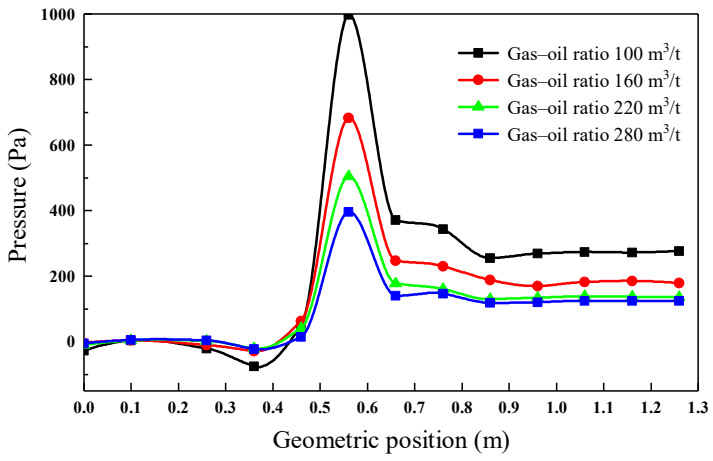

Figure 7. Effect of the gas–oil ratio on the axial pressure distribution of the cylindrical cyclone.

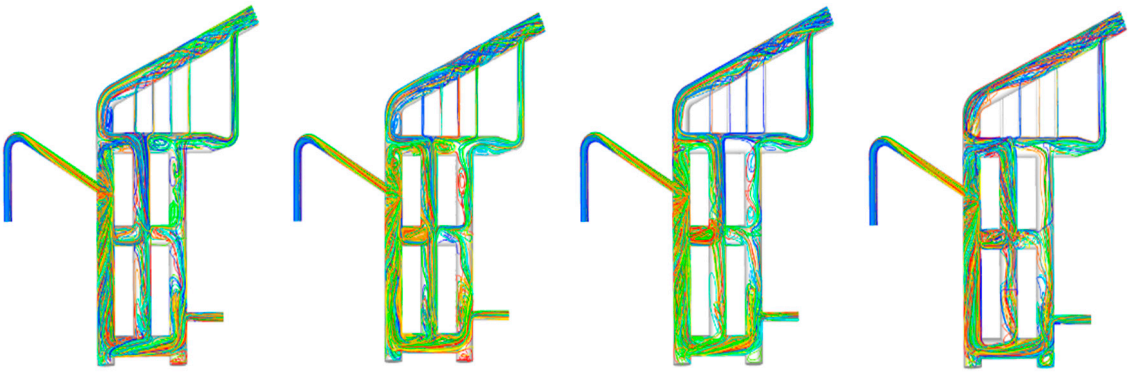

Figure 8. Effect of the gas–oil ratio on the gas–liquid separation flow field characteristics. (**a**) 100 m^3/t; (**b**) 160 m^3/t; (**c**) 220 m^3/t; (**d**) 280 m^3/t.

3.3.2. Separation Performance

The gas–liquid separation effect of the separator under the influence of the gas–oil ratio is shown in Table 5. The water cut was set to 40%, the flow rate was set to 20 m/s, the gasoline ratio increased, and the separation efficiency was reduced. When the gas–oil ratio was 220 m^3/t, the separation efficiency of the separator was less than 60%, and the separation pressure drop also reduced with the increase in the gas–oil ratio. This phenomenon was also consistent with the above understanding of the effect of the water cut on the separation performance.

Table 5. Effect of the gas–oil ratio on the gas–liquid separation performance.

Gas–Oil Ratio, m^3/t	Separation Efficiency, %	Separation Pressure Drop, Pa
100	67.15	4570
160	65.94	3078
220	59.68	2395
280	57.86	1904

3.4. Optimization of the GLCC Structure

The optimization method of the GLCC was roughly the same, either improving the geometry of the separator by analyzing the flow field characteristics inside the separator or introducing pre-separation to improve the separation performance. In terms of the optimization of the inlet angle of the separator, it is generally believed that the optimal angle is 27° [8,16,17]. However, factors such as the cyclone main diameter and multistage separation have a significant impact on the separation performance, and the improvement and optimization of these aspects have not yet fully reached a consensus [30–34].

After the gas–liquid mixture flow conditions were considered, the separation performance of the separator was evaluated and improved. Furthermore, the separation performance of the separator was also improved after the geometric structure was optimized. For the wellhead multistage bundle gas–liquid separator, the largest feature was multi-bundle secondary separation. The number of secondary separation bundles in the separator was four, and the diameter was 26 mm. In the simulation process, when the diameter remained unchanged, the number was increased to six, and when the number remained unchanged, the diameter was increased to 40 mm. The flow field characteristics are shown in Figure 9.

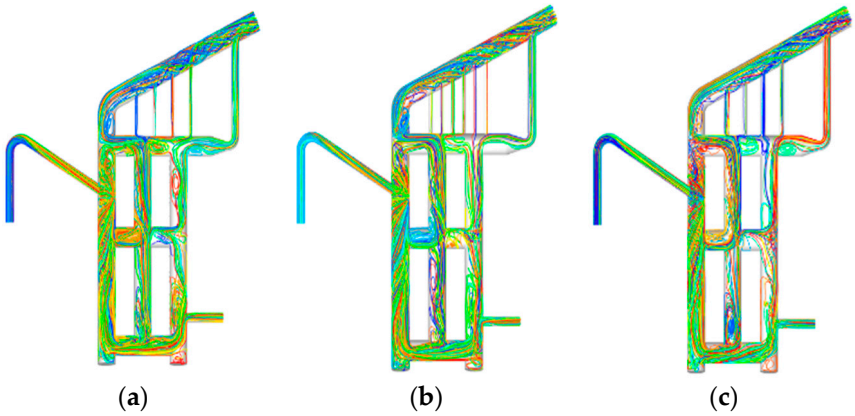

Figure 9. Flow field characteristics with different parameters of secondary separation tube bundles. (**a**) Four branches and 26 mm; (**b**) Six branches and 26 mm; (**c**) Four branches and 40 mm.

The increase in the number of secondary separation bundles obviously improved the effect of secondary separation, reduced the intensity of disturbance to the flow field in the gas-gathering tube, caused the cyclonic characteristics to disappear, and improved the stability of the flow field in the gas-gathering tube. However, at the same time, with the increase in the number of bundles, the turbulence to the flow field in the gas separation elbow increased to some extent due to the increase in branches. The change in bundle diameter also affected the separation efficiency. Compared with the diameter of 26 mm, the gas–liquid separation efficiency was increased by 5% when the diameter was 40 mm. It can be seen from the flow trajectory of the flow field that when the diameter of the bundle was small, it restricted the flow of the liquid phase down the wall of the separation tube during the secondary separation, which affected the amount of gas in the bundle for gas–liquid separation and reduced the separation efficiency. When the bundle diameter increased, the flow field trajectory of liquid phase droplets in the secondary separation bundle significantly improved, the turbulent degree of the gas separation elbow flow field reduced, and the separation efficiency improved. Therefore, the number and diameter of secondary separation fine tube bundles were increased at the same time, and the separation efficiency was further improved.

4. Conclusions

A numerical simulation method was used, and the performance of the wellhead multistage bundle gas–liquid separator was evaluated. The laws of water cut, flow rate, and gas–oil ratio affecting the separation performance were obtained.

(1) When the gas–oil ratio and flow rate were the same and the water cut was increased, the pressure drop required for separation increased, the uniformity and stability of the separation flow field improved, and the gas–liquid separation performance improved. Compared with a water cut of 30%, the separation efficiency of a 50% water cut increased by 5.88%.

(2) When the gas–oil ratio and water cut were the same and the flow rate was increased, the swirl effect of the primary separation was enhanced, and the pressure required for vortex separation at the inlet increased, but the disturbance to the overall separation flow field of the separator was also enhanced, and the irregularity of the streamline trajectory was also strengthened. Under the simulation condition of a flow rate of 15 m/s, a separation efficiency of more than 70% was obtained.

(3) When the flow rate and water cut were the same and the gas–oil ratio was increased, the pressure of the separation flow field reduced, and the stability of the flow field was enhanced. However, when the gas–oil ratio continued to increase from 160 m^3/t, the flow field trace density of the secondary separation bundle reduced continuously, and the separation efficiency under simulated conditions was less than 60%.

(4) Secondary separation affected the overall separation efficiency of the separator. When the number and diameter of the secondary separation bundles were improved, the flow field trajectory of liquid phase droplets in the secondary separation bundle also tended to be dense, further enhancing the stability of the flow field in the gas phase collection tube; the separation efficiency was significantly improved.

Author Contributions: X.Z. performed all the modeling and the simulations. X.Q. prepared the manuscript. S.W. proofread and edited the manuscript. The whole work was supervised by Y.L. All authors have read and agreed to the published version of the manuscript.

Funding: National Natural Science Foundation of China (Grant No. 52074090).

Institutional Review Board Statement: Not applicable.

Informed Consent Statement: Not applicable.

Data Availability Statement: The data presented in this study are available in article.

Acknowledgments: This work presented in this paper was financially supported by the National Natural Science Foundation of China (Grant No. 52074090).

Conflicts of Interest: The authors declare no conflict of interest.

Nomenclature

$\vec{F}$	volume force, N
$\dot{m}$	mass change rate of the mixture, kg/s
N_0	the number of droplets at the primary separation inlet, pcs
N_r	the number of droplets at the gas phase outlet, pcs
$\vec{vdr}, k$	drift velocity of phase k, m/s
$\vec{v_k}$	mass velocity of phase k, m/s
$\vec{v_m}$	mass average velocity of the mixture, m/s
α_k	volume fraction of phase k, %
η	separation efficiency, %
μ_m	viscosity of the mixture, Pa/s
ρ_m	density of the mixture, kg/m^3
ρ_k	density of phase k, kg/m^3

References

1. Wang, Y.; Chen, J.; Ye, S.; Yue, T.; Yang, Y.; Han, M. Calculation model of overflow pressure drop in gas-liquid cylindrical cyclone. *Acta Pet. Sin.* **2021**, *37*, 88–99.
2. Wang, Y.Q.; Li, X.; Lu, J. Experimental study and numerical modeling of boron transport in reservoir and its influence on seawater-breakthrough calculation. *SPE Reserv. Eval. Eng.* **2021**, *24*, 292–309.
3. Liu, Y. *Oil and Gas Gathering and Transferring*; Pet. Ind. Press: Beijing, China, 2015; pp. 222–228.
4. Srinivas, S.K.; Ram, S.M.; Ovadia, S. Analysis of gas-liquid cylindrical cyclone separator with inlet modifications using fluid-structure interaction. *J. Energy Resour. ASME* **2020**, *142*, 042003.
5. Luo, X.; Ren, J.; Chen, T.; Wang, Y.; Lü, Y.; He, L. Influence of slug flow on flow fields in a gas-liquid cylindrical cyclone separator: A simulation study. *Chin. J. Chem. Eng.* **2020**, *28*, 2075–2083.
6. Srinivas, S.K.; Ram, S.M.; Ovadia, S. Numerical Analysis of Flow Behavior in Gas-Liquid Cylindrical Cyclone (GLCC) Separators With Inlet Design Modifications. *J. Energy Resour ASME* **2021**, *143*, 093005.
7. Hreiz, R.; Lainé, R.; Wu, J.; Lemaitre, C.; Gentric, C.; Fünfschilling, D. On the effect of the nozzle design on the performances of gas-liquid cylindrical cyclone separators. *Int. J. Multiphas. Flow* **2014**, *58*, 15–26.
8. Wang, Y.; Chen, J.; Yang, Y.; Han, M.; Zhou, Y.; Ye, S.; Yan, C.; Yue, T. Experimental and numerical performance study of a downward dual-inlet gas-liquid cylindrical cyclone (GLCC). *Chem. Eng. Sci.* **2021**, *238*, 116595.
9. Srinivas, S.K.; Ram, S.M.; Ovadia, S. Structural Integrity Analysis of Gas-Liquid Cylindrical Cyclone (GLCC) Separator Inlet. *J. Energy Resour ASME* **2018**, *140*, 052905.
10. Liu, Y.; Chen, S.; Guan, B. Layout optimization of oil-gas gathering and transportation system in constrained three-dimensional space. *Chin. Sci. Bull.* **2020**, *65*, 834–846.
11. Wang, Z.H.; Liu, X.Y.; Luo, H.; Peng, B.L.; Sun, X.T.; Liu, Y.; Rui, Z.H. Foaming properties and foam structure of produced liquid in alkali/surfactant/polymer flooding production. *J. Energy Resour. Technol.* **2021**, *143*, 103005.

12. Luo, X.; Gao, Q.; Liu, M.; Yang, L.; He, L. Separation characteristics of axial-flow gas-liquid cyclone separator. *Acta Pet. Sin. (Pet. Processing Sect.)* **2020**, *36*, 592–599.
13. Yang, Z.; He, L.; Tian, Y.; Luo, X. Numerical simulation of separation characteristics of heavy oil in cylindrical cyclone separator. *Oil Gas Storage Transp.* **2020**, *39*, 0319–0325.
14. Torstein, T.K.; Christian, H.; Olav, E. Feedback Linearizing Control of a Gas-Liquid Cylindrical Cyclone. *IFAC PapersOnLine* **2017**, *50*, 13121–13128.
15. Zhang, Y.; Xing, L.; Jiang, M.; Zhang, Y. Effects of discrete phase particle size on hydrocyclone separation performance. *J. Northeast. Pet. Univ.* **2018**, *42*, 109–116.
16. Juan, C.B.; Eduardo, P.; Nicolas, R. Computational Fluid Dynamics Modeling of Gas-Liquid Cylindrical Cyclones, Geometrical Analysis. *J. Energy Resour. Technol.* **2018**, *140*, 092003.
17. Le, V.S. Influence of inlet angle on flow pattern and performance of gas-liquid cylindrical cyclone separator. *Part. Sci. Technol.* **2017**, *35*, 555–564.
18. Amirhosein, G.; Mehrzad, S.; Mohammad, M.H. A numerical scheme for optimizing gas liquid cylindrical cyclone separator. *Proc. Inst. Mech. Eng.* **2017**, *231*, 836–848.
19. Luo, H.J.; Wen, J.B.; Lv, C.L.; Wang, Z.H. Modeling of viscosity of unstable crude oil–water mixture by characterization of energy consumption and crude oil physical properties. *J. Pet. Sci. Eng.* **2022**, *212*, 110222.
20. Yang, W.P.; Fu, C.L.; Du, Y.J.; Xu, K.; Balhoff, M.T.; Weston, J.; Lu, J. Dynamic contact angle reformulates pore-scale fluid-fluid displacement at ultralow interfacial tension. *SPE J.* **2021**, *26*, 1278–1289.
21. Zhu, C.; Liu, X.; Xu, Y.; Liu, W.; Wang, Z. Determination of boundary temperature and intelligent control scheme for heavy oil field gathering and transportation system. *J. Pipeline Sci. Eng.* **2021**, *1*, 407–418.
22. Chang, P.; Hu, T.; Wang, L.; Chang, S.; Wang, T.; Wang, Y. Numerical Simulation on Structure Optimization of Liquid-Gas Cylindrical Cyclone Separator. *Int. J. Chem. Eng.* **2016**, *2016*, 1–9.
23. Wang, H.; Xu, Y.; Shi, B.; Zhu, C.; Wang, Z. Optimization and intelligent control for operation parameters of multiphase mixture transportation pipeline in oilfield: A case study. *J. Pipeline Sci. Eng.* **2021**, *1*, 367–378.
24. Sun, Y.; Cao, X.; Liang, F.; Sun, S. Numerical simulation and experimental verification of a gas-liquid two-phase flow tube separator. *Oil Gas Storage Transp.* **2018**, *37*, 885–890.
25. Zhong, H.Y.; He, Y.Y.; Yang, E.L.; Bi, Y.B.; Yang, T.B. Modeling of microflow during viscoelastic polymer flooding in heterogenous reservoirs of Daqing Oilfield. *J. Pet. Sci. Eng.* **2022**, *210*, 110091.
26. Zhu, W.; Hu, L.; Zhang, X. The effects of the lower outlet on the flow field of small gas-liquid cylindrical cyclone. *Proc. Inst. Mech. Eng. Part C J. Mech. Eng. Sci.* **2019**, *233*, 1262–1270.
27. Zhang, J.; Pang, Y.; Li, Z.; Wang, Z. Effect of Dissolved-Air Flotation on Flow Field Characteristics of Produced Water in Settlement Separation Process. *J. Petrochem. Univ.* **2021**, *34*, 72–79.
28. Yang, L.; Zhang, J.; Ma, Y.; Xu, J.; Wang, J. Experimental and numerical study of separation characteristics in gas-liquid cylindrical cyclone. *Chem. Eng. Sci.* **2020**, *214*, 115362.
29. Liu, J.; Qiang, Y.; Mian, M.; Xu, W.; Du, E. Rheology of soft and rigid micro particles in curved microfluidic channels. *Mech. Biol. Syst. Mater.* **2017**, *6*, 83–87.
30. Wu, K.; Zhang, H.; Yang, Y.; Liu, X. Strength matching factor of pipeline girth weld designed by reliability method. *J. Pipeline Sci. Eng.* **2021**, *1*, 298–307.
31. Mann, H.; Roloff, C.; Hagemeier, T.; Thévenin, D.; Tomas, J. Model-based experimental data evaluation of separation efficiency of multistage coarse particle classification in a zigzag apparatus. *Powder Technol.* **2017**, *313*, 145–160.
32. Niazi, H.; Wang, S.D.; Lamborn, L.; Eadie, R.; Chen, W.X.; Zhang, H. Effects of load interactions on the onset of stage two of high pH stress corrosion cracking. *J. Pipeline Sci. Eng.* **2021**, *1*, 122–136.
33. Li, Z.; Liang, Y.; Liao, Q.; Zhang, B.; Zhang, H. A review of multiproduct pipeline scheduling: From bibliometric analysis to research framework and future research directions. *J. Pipeline Sci. Eng.* **2021**, *1*, 395–406.
34. Krebs, T.; Schroen, C.P.G.H.; Boom, R.M. A microfluidic study of oil-water separation kinetics. *WIT Trans. Eng. Sci.* **2012**, *74*, 427–438.